J|A|C|S COMMUNICATIONS

Published on Web 09/29/2009

Dip-Pen Lithography of Ferroelectric $PbTiO_3$ Nanodots

Jong Yeog Son,[†] Young-Han Shin,[†] Sangwoo Ryu,[†] Hyungjun Kim,[‡] and Hyun M. Jang*,[†]

Department of Materials Science and Engineering, and Division of Advanced Materials Science, Pohang University of Science and Technology, Pohang 790-784, Korea, and School of Electrical and Electronic Engineering, Yonsei University, Seoul 120-749, Korea

Received August 24, 2009; E-mail: hmjang@postech.ac.kr

Ferroelectric random access memory (FeRAM) is one of the promising nonvolatile memory devices that shows simple device structures and fast operation.[1−8] Recently, device scale-down has been accelerated with the demands of high-performance and high-density data storage for the management of high-quality media. In order to achieve a high density of FeRAM as a next-generation memory, a ferroelectric capacitor must be as small as possible.[6−8] As a simple approach to the fabrication of ferroelectric nanostructures, randomly positioned nanodots are commonly obtained using precursor sols.[17,18] As this method produces nanodots with various sizes, it is not suitable for FeRAM applications. On the other hand, the nanodot fabrication technique based on anodizing aluminum oxide (AAO) nanotemplates enables us to form ferroelectric nanocapacitor arrays having a high density of ~0.2 Tbit/in.^{2} (see refs 5, 7, 8). However, this approach also hardly seems to be adapted to the top-down manner of the established memory fabrication techniques because this template-based fabrication process cannot control the position of the nanostructure at a desired place in FeRAM applications.[1,2] Thus, it is highly desirable to position a ferroelectric nanodot at a desired place, which can be well-adapted to the established memory fabrication technology.

Dip-pen nanolithography (DPN), which enables us to form nanopatterns with various molecules at desired places, is one of noble atomic force microscopy (AFM) techniques that utilize both electric force microscopy (EFM) and piezoresponse force microscopy (PFM).[9−15] DPN technology originated from the patterning of 1-octadecanethiol polymers by Piner et al.[9] Because of the capability of AFM to control position, DPN technology has produced diverse nanopatterns with various materials such as metals, semiconductors, proteins, cells, and even viruses.[9−16] Thus, the DPN technology is expected to be one of the feasible solutions for the realization of position-controlled ferroelectric nanostructures in FeRAM applications. In spite of the expectation, however, this technology has not been successfully applied to the fabrication of ferroelectric nanostructures. In this study, we report the fabrication of ferroelectric $PbTiO_3$ (PTO) nanodots with various sizes ranging from 37 to 200 nm using DPN technology. The ferroelectric PTO nanodots exhibit well-defined canonical ferroelectric responses, as confirmed by PFM and EFM studies.

Unlike DPN involving polymers,[9,19] we adopted sequential drying and annealing processes for the fabrication of ferroelectric PTO nanodots using DPN technology. In Figure 1, we schematically depict the DPN process of ferroelectric PTO nanodots. For the DPN of PTO nanodots, we used a PbO-excess precursor sol modified with a low-viscosity alcohol. We first formed PTO-

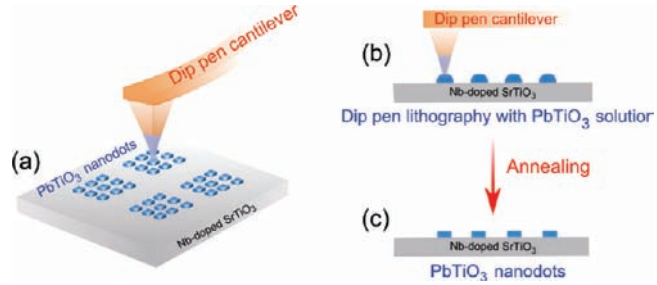

Figure 1. Schematic drawings illustrating the dip-pen nanolithography (DPN) of ferroelectric $PbTiO_3$ (PTO) nanodots. (a) Patterns of PTO nanodots formed by DPN. (b) Formation of a nanopattern using a PTO precursor sol on the surface of Nb-doped $SrTiO_3$ by DPN. (c) To obtain highly crystallized PTO nanodots, an annealing process is carried out after the lithography of the PTO nanopattern is performed.

precursor sol nanodots on a Nb-doped $SrTiO_3$ (STO) substrate (Figure 1b). To elaborate the DPN process, we also used a Nb-doped STO substrate that had an atomically flat surface with well-aligned terraces formed by HF treatment with annealing. After the deposition, we slowly dried these precursor sol nanodots for a week at room temperature. For the crystallization of ferroelectric perovskite PTO, we annealed these nanodots under an oxygen atmosphere at 650 °C for 1 min by rapid thermal annealing. Structural and ferroelectric characterizations of the PTO nanodots were then made by AFM, PFM, and EFM measurements in conjunction with a high-resolution transmission electron microscopy (HR-TEM, JEM-2200FS) study.

The size of the nanodots was controlled by suitably adjusting the dip-pen deposition time. We were able to obtain various sizes of ferroelectric nanodots, as shown in the AFM images (Figure 2a). Interestingly, these DPN nanodots are square-shaped, indicating a high degree of crystallinity. At the bottom background region, well-aligned terraces of the Nb-doped STO crystalline substrate are discernible, where the Nb-doped STO is used as a bottom electrode of the PTO nanodot capacitor. In addition, this material showed an atomically flat surface, with a surface roughness of less than 0.2 nm. Thus, it provides an optimum surface for the DPN of ferroelectric PTO nanodots. Sizes and thicknesses of the nanodot increase with the dip-pen deposition time (Figure 2b,c). During the initial deposition period, the size of the PTO nanodot increases rapidly. The nanodot is saturated in its lateral dimension at ~230 nm.

Magnified AFM images of the minimum-sized DPN nanodot are presented in Figure 3a,b. We confirmed the epitaxial growth of the minimum-sized nanodot with a single-domain structure by HR-TEM (Figure 3c). From the HR-TEM lattice image, we estimated the *c*/*a* ratio of the minimum-sized PTO nanodot to be 1.08, which is larger than that of the unstrained bulk PTO

[†] Department of Materials Science and Engineering and Division of Advanced Material Science, Pohang University of Science and Technology.
[‡] School of Electrical and Electronic Engineering, Yonsei University.

10.1021/ja906871b CCC: $40.75

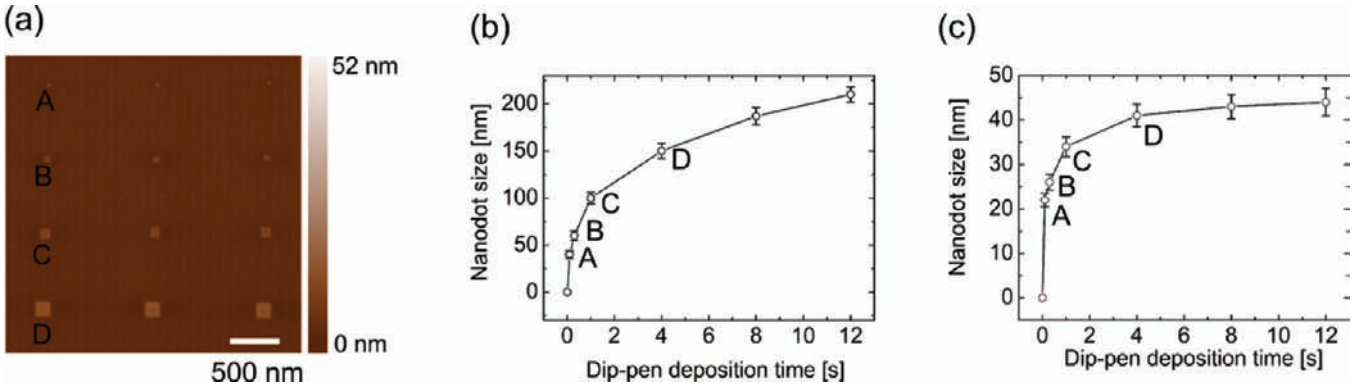

Figure 2. AFM images of PTO nanodots formed by DPN. (a) Array of PTO nanodots formed by DPN using various dip-pen deposition times. (b) Plot of the lateral dimension of the PTO dot as a function of the dip-pen deposition time. (c) Plot of the thickness of the PTO nanodot as a function of the dip-pen deposition time.

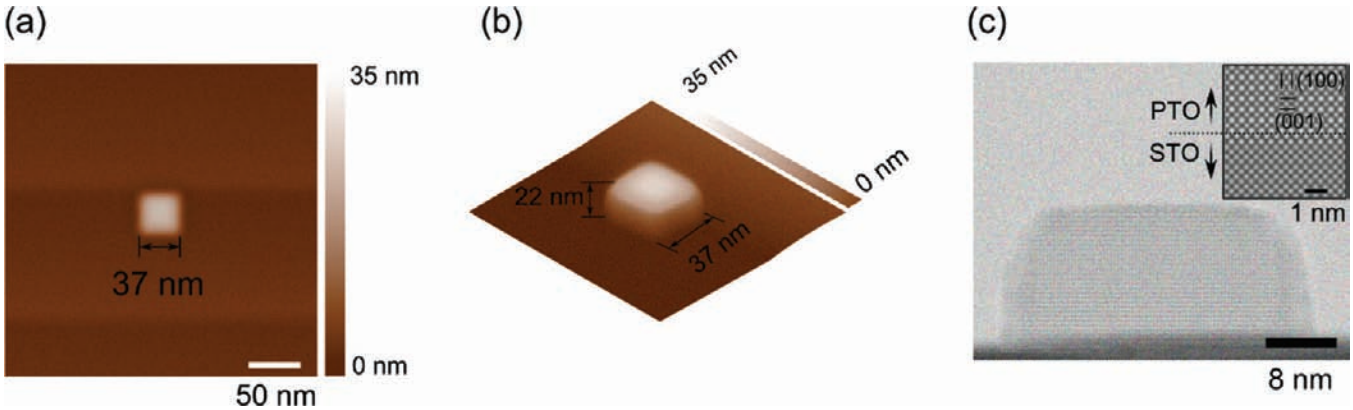

Figure 3. Minimum-sized PTO nanodot with a lateral dimension of 37 nm. (a) AFM image of the minimum-sized PTO nanodot. (b) Three-dimensional AFM image of the minimum-sized PTO nanodot. The thickness of this minimum-sized nanodot is ~22 nm. (c) HR-TEM image of the minimum-sized PTO nanodot. The *c*/*a* ratio (i.e., tetragonality) was estimated to be 1.08.

(1.06), suggesting a highly strained nanostructure grown along the polar *c* axis of the tetragonal 4*mm* (C_{4v}) symmetry. The minimum-sized PTO nanodot is square-shaped with a lateral dimension of 37 nm and a thickness of ~22 nm. This minimum-sized nanodot is capable of showing a maximum storage density of ~0.5 Tbit/in.^{2} for FeRAM applications. This value of the storage density is higher than that of the ferroelectric array fabricated by the AAO membrane technique.[7] Moreover, we note that this DPN technique is capable of positioning a nanodot at a desired place. In the DPN process for ferroelectric PTO nanodots, we used a DPN tip with a radius slightly smaller than 10 nm. However, we would be able to obtain a nanodot substantially smaller than the present minimum-sized PTO nanodot by employing a sharper DPN tip. This is because the size of DPN nanodot is controlled primarily by the sharpness of the DPN tip.[12]

We have further investigated the ferroelectric properties of the minimum-sized PTO nanodot by employing PFM and EFM. For this purpose, we used a platinum-coated Si_3N_4 cantilever with a conducting tip having a radius of ~20 nm. Thus, the resolution was not high enough to obtain a good AFM image of the minimum-sized nanodot, though the AFM image was obtained using contact AFM mode (Figure 4b). In Figure 4c, we present a PFM image of the minimum-sized PTO nanodot. The PFM image is featured by a dark-colored region surrounded with a bright region.

We also obtained a typical piezoelectric hysteresis loop from the minimum-sized PTO nanodot by PFM at a measurement frequency of 10 kHz. The hysteresis loop showed a coercive voltage of ~1.0 V and an effective remanent piezoelectric constant of ~100 pm/V (Figure 4d). For the A, B, C, and D nanodots shown in Figure 2a,b, the d_{33} value of the PFM hysteresis loop decreased while the coercive electric field increased with the lateral size (see the Supporting Information). The coercive electric field of ferroelectric nanodots increases, in general, with decreasing thickness or increasing lateral size, and the PFM signal is also closely related to the aspect ratio of a nanodot.[20−23] Thus, the present PFM results well reflect the ferroelectric size effect associated with the scale-down.[20−23]

We confirmed the ferroelectric switching properties of the minimum-sized PTO nanodot by switching and reading a ferroelectric domain based on the EFM study (Figure 4e,f). During the switching, it is expected that a high electric field is applied to the minimum-sized nanodot because of its small thickness (~22 nm) in conjunction with a sharp EFM tip.[24] To polarize the ferroelectric domain formed on the surface of the Nb-doped STO electrode, we applied a bias of +0.5 V to the minimum-sized PTO nanodot. We subsequently flipped this domain with a bias voltage of −0.5 V. The EFM image of the switched ferroelectric domain revealed a positive surface potential, indicating that the ferroelectric polarization is oriented along the field direction (i.e., vertical to the surface of the minimum-sized nanodot; 4e). This polarization was then readily flipped by applying a bias of +0.5 V. According to the EFM image, the ferroelectric domain is perfectly flipped, ending up with a negative surface potential, which again implies that the polarization is oriented vertical to the bottom electrode surface

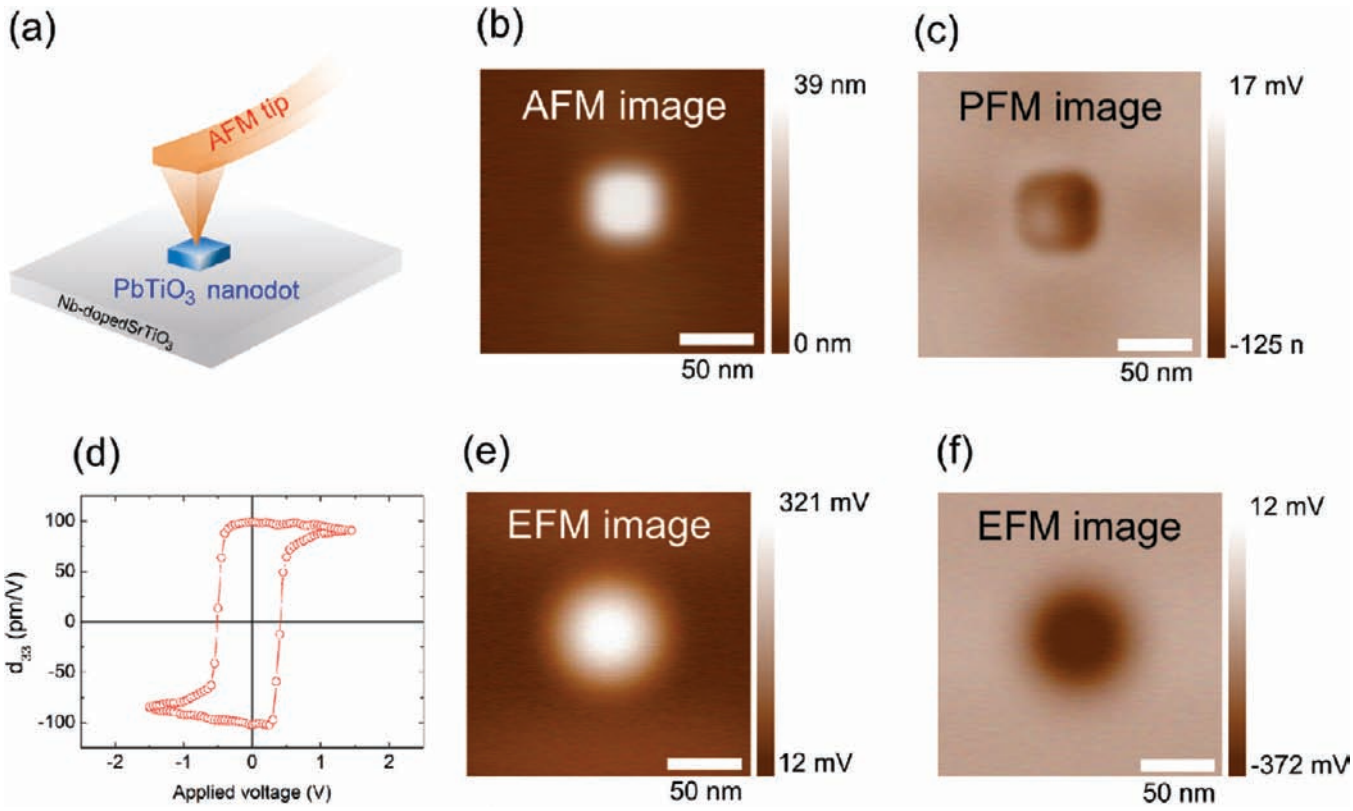

Figure 4. PFM and EFM measurements of a. PTO nanodot formed by DPN. (a) Electrical contact of a PTO nanodot with an AFM tip for PFM and EFM measurements. (b) Image of the PTO nanodot obtained by AFM with a Pt-coated Si_3N_4 cantilever. (c) PFM image of the PTO nanodot. (d) Value of d_{33} for the minimum-sized PTO nanodot plotted as a function of the applied voltage. (e) EFM image of the PTO nanodot after switching with a bias of −0.5 V. (f) EFM image of the PTO nanodot after switching with a bias of +0.5 V.

(Figure 4f). We confirmed a reproducible switching behavior of the ferroelectric polarization up to 1000 cycles. From the domain switching and the reading with EFM, we are able to obtain quantitative information on the switching characteristics of the PTO nanodot needed for FeRAM applications.

In summary, we have carried out DPN experiments to form ferroelectric PTO nanodots using a suitably prepared PTO precursor sol. The ferroelectric PTO nanodots exhibited a size increment from 37 to 200 nm for deposition times between 0.1 and 10 s. The minimum-sized ferroelectric PTO nanodot is characterized by a single domain with a lateral dimension of 37 nm and a thickness of ∼22 nm. We demonstrated ferroelectric switching characteristics of the minimum-sized nanodot using PFM and EFM. The minimum-sized PTO nanodot is estimated to show a maximum storage density of ∼0.5 Tbit/in.^{2}, which is suitable for high-density FeRAM applications.

Acknowledgment. This work was supported by the Brain Korea 21 Project 2008 and the Korea Research Foundation Grant (MOEHRD) under Contracts KRF-2007-314-C00111 and KRF-2008-313-C00309. This research was also supported by the WCU (World Class University) Program of the Ministry of Education, Science and Technology (Project R31-2008-000-10059-0), Republic of Korea, and the Korea Science and Engineering Foundation (KOSEF) (Grant R01-2007-000-20143-0).

Supporting Information Available: Frequency dependence of polarization and structural data. This material is available free of charge via the Internet at http://pubs.acs.org.

References

(1) Scott, J. F.; Paz de Araujo, C. A. *Science* **1989**, *246*, 1400–1405.
(2) Paz de Araujo, C. A.; Cuchiaro, J. D.; McMillan, L. D.; Scott, M. C.; Scott, J. F. *Nature* **1995**, *374*, 627–629.
(3) Auciello, O.; Scott, J. F.; Ramesh, R. *Phys. Today* **1998**, *51*, 22–27.
(4) Park, B. H.; Kang, B. S.; Bu, S. D.; Noh, T. W.; Lee, J.; Jo, W. *Nature* **1999**, *401*, 682–684.
(5) Sun, T.; Pan, Z.; Dravid, V. P.; Wang, Z.; Yu, M.-F.; Wang, J. *Appl. Phys. Lett.* **2006**, *89*, 163117.
(6) Scott, J. F. *Science* **2007**, *315*, 954–959.
(7) Lee, W.; Han, H.; Lotnyk, A.; Schubert, M. A.; Senz, S.; Alexe, M.; Hesse, D.; Baik, S.; Gosele, U. *Nat. Nanotechnol.* **2008**, *3*, 402–407.
(8) Hu, Z.; Tian, M.; Nysten, B.; Jonas, A. M. *Nat. Mater.* **2009**, *8*, 62–67.
(9) Piner, R. D.; Zhu, J.; Xu, F.; Hong, S.; Mirkin, C. A. *Science* **1999**, *283*, 661–663.
(10) McKendry, R.; Huck, W. T. S.; Weeks, B.; Fiorini, M.; Abell, C.; Rayment, T. *Nano Lett.* **2002**, *2*, 713–716.
(11) Lee, K.-B.; Lim, J.-H.; Mirkin, C. A. *J. Am. Chem. Soc.* **2003**, *125*, 5588–5589.
(12) Salaita, K.; Wang, Y.; Mirkin, C. A. *Nat. Nanotechnol.* **2007**, *2*, 145–155.
(13) Li, B.; Goh, C. F.; Zhou, X.; Lu, G.; Tantang, H.; Chen, Y.; Freddy, C. X.; Boey, Y. C.; Zhang, H. *Adv. Mater.* **2008**, *20*, 4873–4878.
(14) Wang, W. M.; Stoltenberg, R. M.; Liu, S.; Bao, Z. *ACS Nano* **2008**, *2*, 2135–2142.
(15) Basnar, B.; Willner, I. *Small* **2009**, *5*, 28–44.
(16) Lee, S.; Lee, S.; Ko, Y.-H.; Jung, H.; Kim, J. D.; Song, J. M.; Choo, J.; Eo, S. K.; Kang, S. H. *Talanta* **2009**, *78*, 608–612.
(17) Ma, J.; Lu, X.; Kan, Y.; Gu, J.; Zhu, J. S. *Integr. Ferroelectr.* **2005**, *73*, 149–156.
(18) Pan, Z.; Donthu, S. K.; Wu, N.; Li, S.; Dravid, V. P. *Small* **2006**, *2*, 274–280.
(19) Huo, F.; Zheng, Z.; Zheng, G.; Giam, L. R.; Zhang, H.; Mirkin, C. A. *Science* **2008**, *321*, 1658–1660.
(20) Shih, W. Y.; Shih, W.-H.; Aksay, I. A. *Phys. Rev. B* **1994**, *50*, 15575.
(21) Alexe, M.; Harnagea, C.; Hesse, D.; Gosele, U. *Appl. Phys. Lett.* **2001**, *79*, 242–244.
(22) Bühlmann, S.; Dwir, B.; Baborowski, J.; Muralt, P. *Appl. Phys. Lett.* **2002**, *80*, 3195–3197.
(23) Anna, N. M.; Sergei, V. S.; Eugene, A. E.; Sergei, V. K. *Phys. Rev. B* **2007**, *76*, 054123.
(24) Tybell, T.; Paruch, P.; Giamarchi, T.; Triscone, J. M. *Phys. Rev. Lett.* **2002**, *89*, 097601.

JA906871B